Supplementary Information

Chemical Disorder Suppresses Thermal Transport through Local Stress Redistribution in $SrTiO_3$-Based High-Entropy Perovskites

Yongheng Li[1], Maomao Liu[2], Hongwei Du[1], Baole Wei[1], Bin Wei*[2], Bonan Zhu*[1,3], Ziheng Lu*[1], Yuanhua Lin[4]

[1]Zhongguancun Institute of Artificial Intelligence, Beijing 100094, China
[2]Henan Key Laboratory of Materials on Deep-Earth Engineering, School of Materials Science and Engineering, Henan Polytechnic University, Jiaozuo 454000, China
[3]School of Aerospace Engineering, Beijing Institute of Technology, Beijing 100081, China
[4]State Key Laboratory of New Ceramics and Fine Processing, School of Materials Science and Engineering, Tsinghua University, Beijing 100084, China

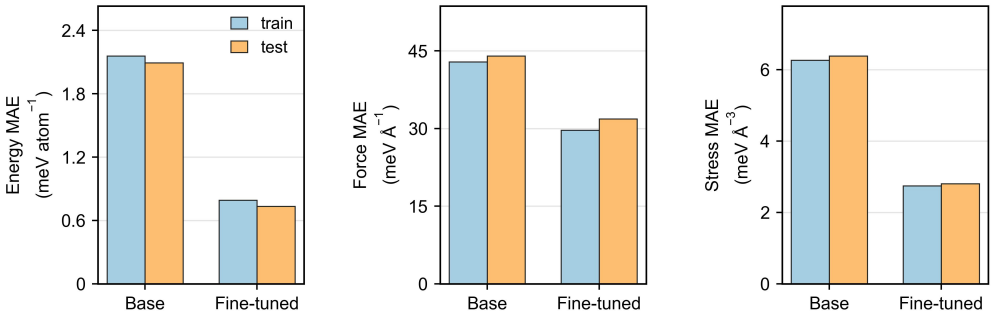

Fig. S1: Validation of MACE fine-tuning for high-entropy $SrTiO_3$ configurations. The comparison between the pretrained and fine-tuned models shows that 615 DFT-labelled structures substantially improve the description of energies, forces and stresses in chemically disordered STO configurations.

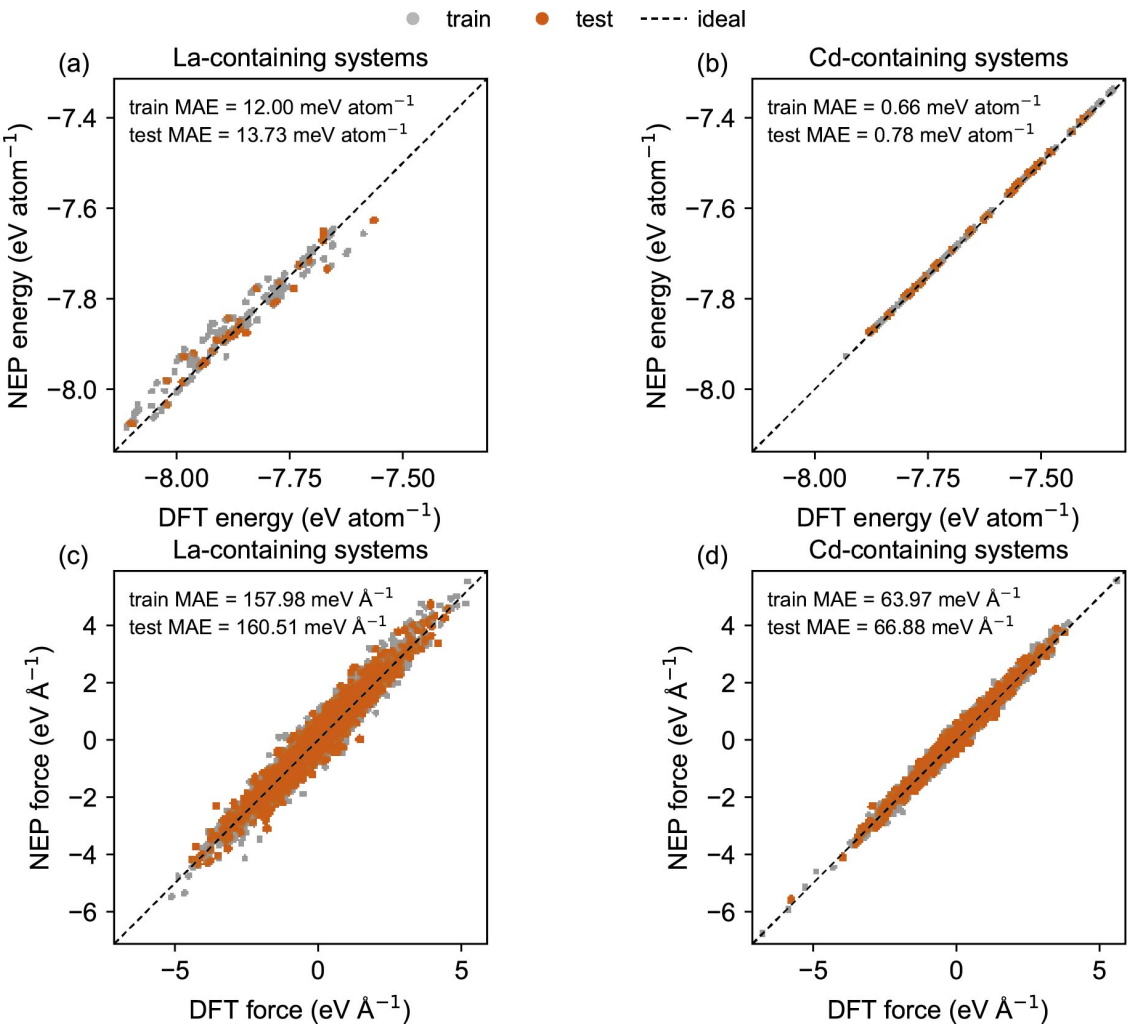

Fig. S2: Direct NEP performance for La- and Cd-containing STO-based chemical spaces. Energy and force parity plots compare DFT reference values with direct NEP predictions for (a,c) La-containing and (b,d) Cd-containing systems. The two models were trained using the same number of DFT-labelled structures and evaluated using the same procedure. Grey and orange points denote training and test data, respectively, and dashed lines indicate ideal agreement. The substantially lower errors for the Cd-containing control show that the large direct-NEP errors obtained for the target La-containing space are not a generic consequence of the dataset size or evaluation procedure.

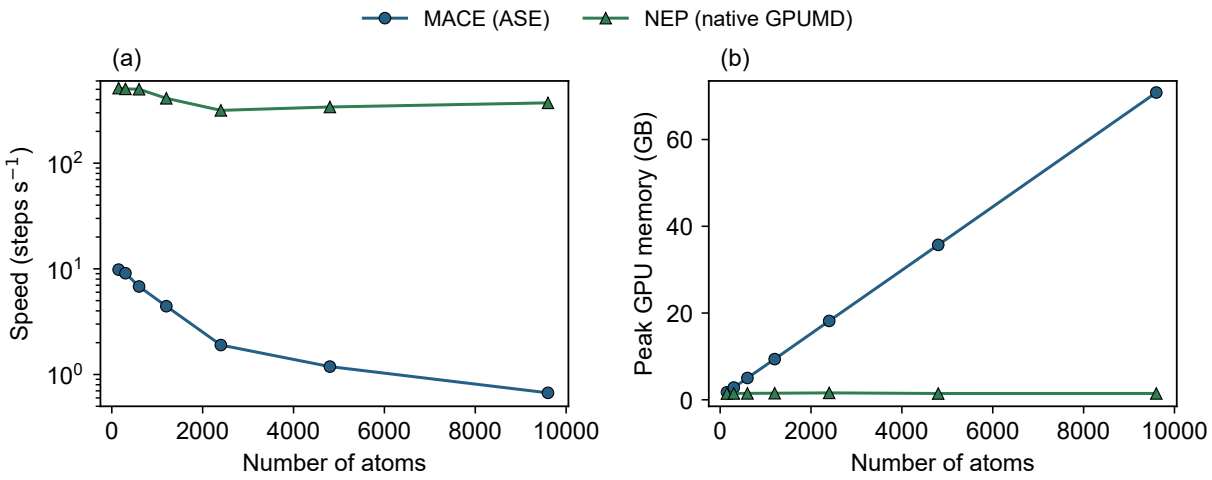

Fig. S3: GPU benchmark for the fine-tuned MACE teacher and distilled NEP using systems containing 150 to 9600 atoms. Both models were run for 50 simulation steps at each system size on an NVIDIA A100-SXM4-80GB GPU. MACE used the CUDA-enabled ASE `MACECalculator` without cuEquivariance, whereas NEP used native GPUMD. (a) Throughput on a logarithmic scale. (b) Incremental peak GPU memory.

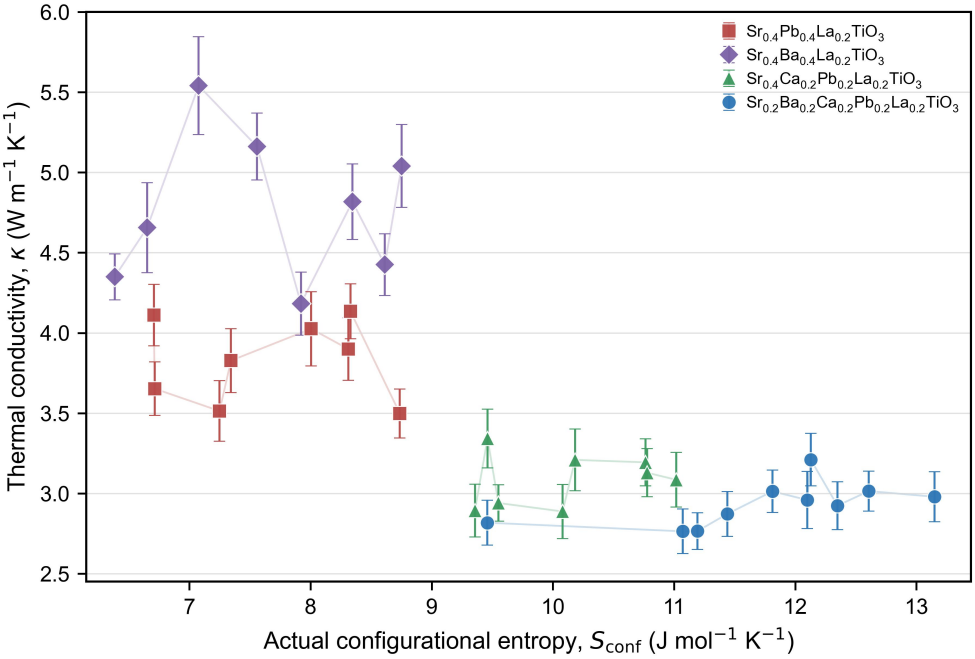

Fig. S4: Effect of A-site short-range order on lattice thermal conductivity. The comparison across representative SRO-sampled structures shows that the conductivity variation induced by A-site arrangement is smaller than the composition-driven trends discussed in the main text.

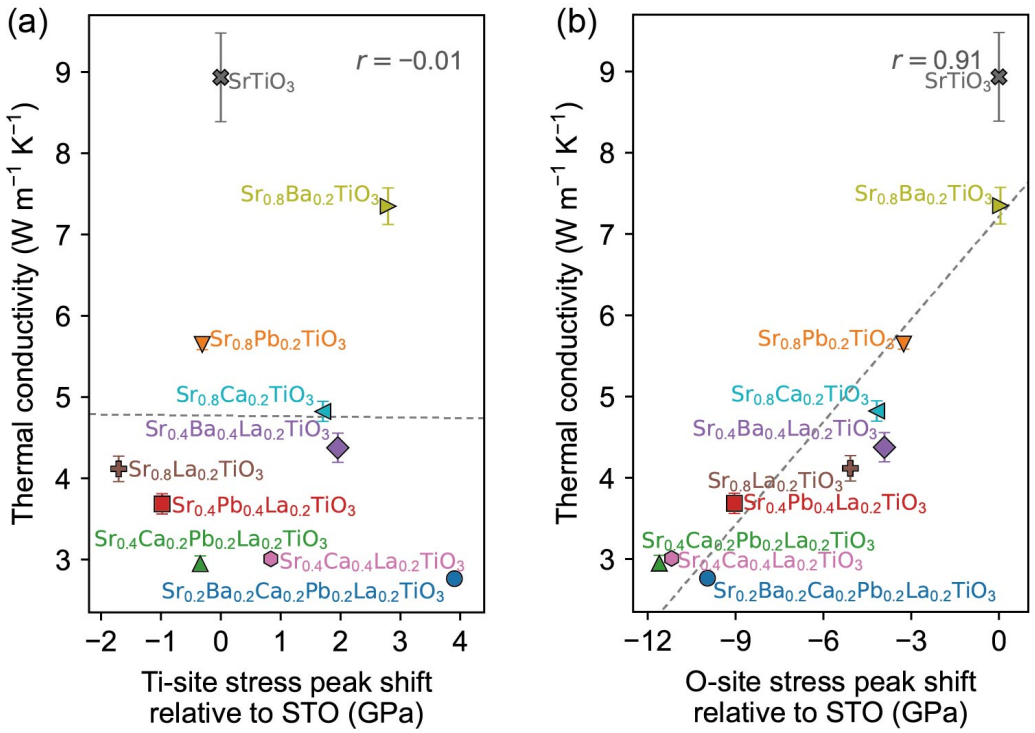

Fig. S5: Site-resolved stress peak shifts and lattice thermal conductivity. For each site type, the instantaneous $s_i(t)$ values were pooled over the relevant atoms and sampled frames, and the normalized distributions were averaged over representative SQS/SRO structures for each composition. (a) Thermal conductivity versus the shift of the dominant Ti-site peak relative to ordered $SrTiO_3$. (b) Thermal conductivity versus the corresponding O-site peak shift. The weak Ti-site correlation ($r = -0.01$) and strong positive correlation with the signed O-site shift ($r = 0.91$) demonstrate that the finite-temperature local stress redistribution is site dependent and is transmitted from the substituted A sublattice into the TiO_6 framework. Pearson coefficients are calculated from the plotted central values, and grey dashed lines are linear guides to the eye.

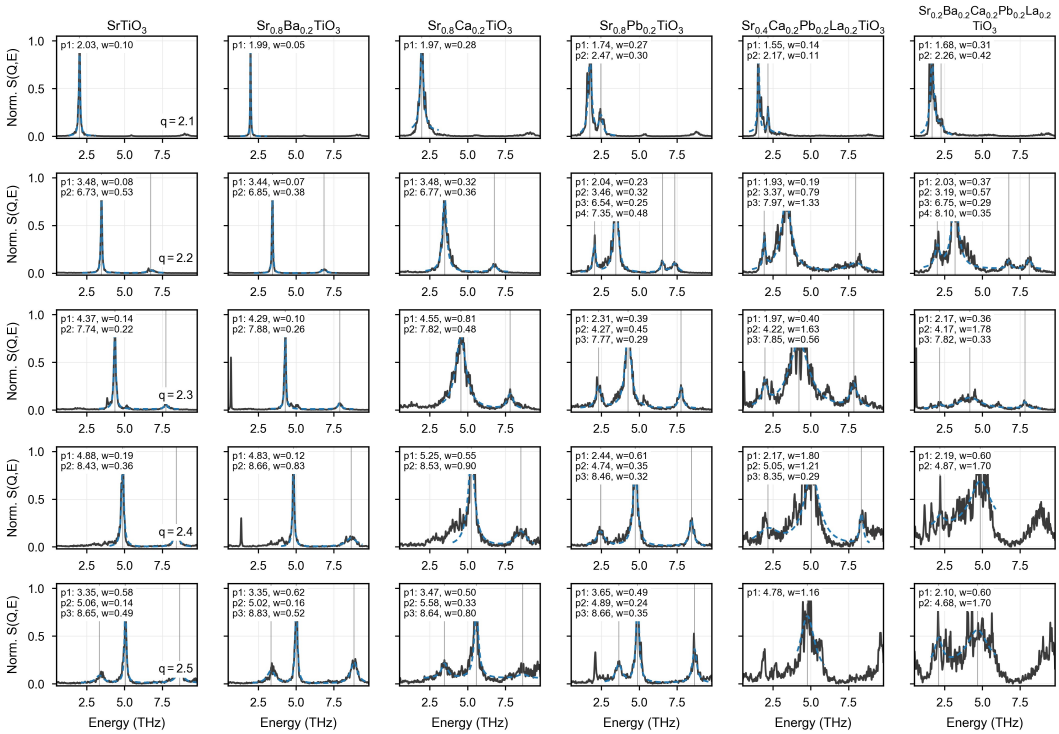

Fig. S6: Representative constant-Q fits used for the peak-to-background spectral analysis. The integrated area of the fitted coherent peak-like phonon components defines R_{peak}, while the integrated area of the fitted diffuse background over the same energy window defines R_{bg}.

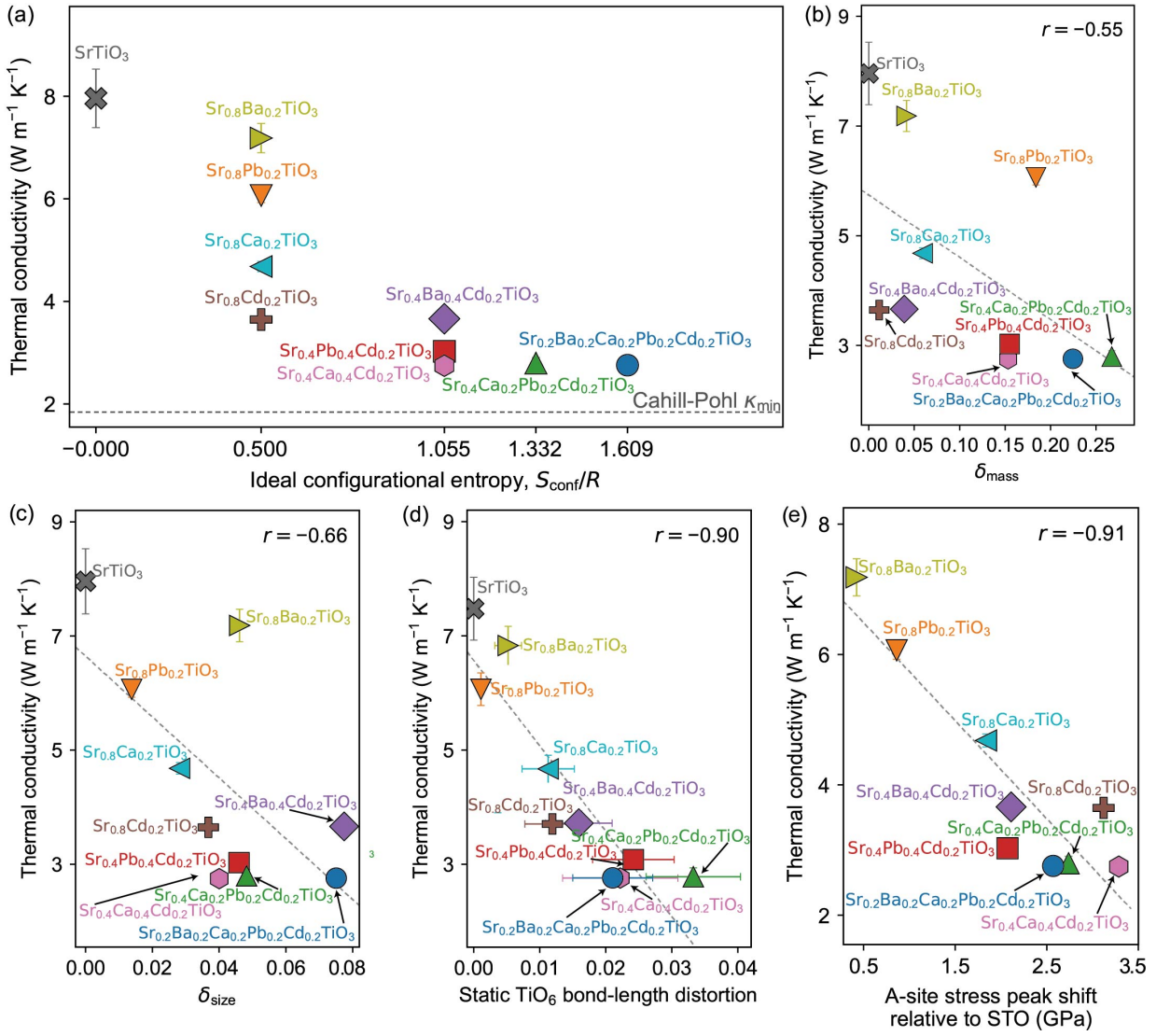

Fig. S7: Descriptor dependence of lattice thermal conductivity in the Cd-containing composition series. (a) Thermal conductivity versus ideal A-site configurational entropy. (b) Thermal conductivity versus A-site mass fluctuation. (c) Thermal conductivity versus A-site ionic-size mismatch. (d) Thermal conductivity versus TiO_6 bond-length distortion. (e) Thermal conductivity versus the A-site stress peak shift relative to ordered $SrTiO_3$. Pearson coefficients are calculated from the plotted central values, and grey dashed lines are linear guides to the eye. The thermal-conductivity, relaxed-structure and stress results were obtained using the NEP model for the Sr/Ca/Ba/Pb/Cd-containing STO systems.